Wideband Equivalent Circuit Model and Parameter Computation of Automotive Ignition Coil Based on Finite Element Analysis

Jia Jin, Wang Quan-di, Yu Ji-hui, Zheng Ya-li

State Key Laboratory of Power Transmission Equipment & System Security and New Technology, Chongqing University, Chongqing 400030, China
twoj1985-163.com@163.com, wangquandi@yahoo.com.cn, yujihui@cqu.edu.cn, yaya9304@163.com

Abstract- This paper presents a coupled field-circuit method to predict the wideband characteristic of ignition coils. A lumped circuit model is proposed, which separates the winding of ignition coil into individual sections. In this circuit model, the capacitance between sections, turn-to-turn series capacitance of each single section and inductance of winding are calculated by Finite Element Analysis (FEA). This parameter identification is based on the energy principle. In addition, this paper analyzes the influence of frequency on the magnetic-flux distribution and the inductance, using the finite-element model with T-Ω formulation. The parameter inductance applied to the circuit model is classified into high frequency inductance and low frequency inductance. Through contrasting the measured and calculated result in frequency and time domain, reliability and feasibility of the presented method in this paper is verified.

Index Terms—Coupled field-circuit method, wideband characteristic, ignition coil, Finite Element Analysis (FEA), T-Ω formulation.

I. INTRODUCTION

Ignition coil acts as a transient voltage transformer in the ignition process [1]. Its function is to convert a low-voltage DC source into a very high and fast transient voltage at the spark plug gap. Due to the primary and secondary coil inductance, stray capacitance, and core eddy current loss, the ignition coil terminal characteristics become more sophisticated than in the stationary state. Thus, it is necessary to couple the finite element analysis (FEA) with an electric circuit model to perform system-level simulation.

In general, there are three main categories of models for a transient voltage transformer. The first type is the winding model, which is based on the multiconductor transmission-line theory (MTL) [2-3]. The second type [4-5] is the terminal or black box model, which provides the terminal characteristics of the transformer and is not necessarily related to a transformer's internal condition. The third type is the physical model; it can model all parts of the transformer in great detail and can be constructed according to equivalent lumped electric circuit parameters [6-7].

It is a crucial problem to correctly extract the equivalent parameters for establishing the wideband circuit model of the transient transformer. Methods for obtaining the parameters include the analytic method [3, 6], experimental method [5] and the numerical method [2, 8] (especially FEA). Because of the high computational accuracy and wide adaptation to complicated physical models, FEA provides the most useful avenue to obtain the stray parameters of transformer and investigate the steel core characteristic depending on the frequency.

A wideband, lumped parameter equivalent circuit model topology for ignition coil is proposed. Then the parameters in the circuit model are presented using electromagnetic finite element analysis. Finally, the measured and simulated frequency- and time-domain results are given and analyzed. These results show that the proposed model accurately predicts the ignition coil terminal responses in the frequency range between 100Hz and 10MHz.

II. COMPUTATIONAL MODEL

The ignition coil 2D cross-section is described in Fig. 1 (a). The primary winding has 150 turns and secondary has 13000 turns. Figure 1 (b) shows a single section of the secondary winding, which consists of hundreds of coated copper wires. The

wires in this secondary section are arranged of approximate 30 layers and 60 turns per layer.

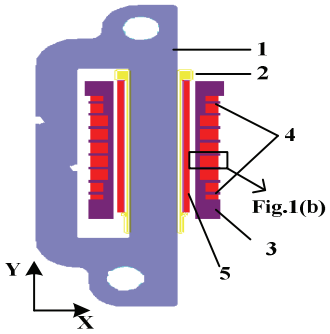

Fig.1(b)

(a)

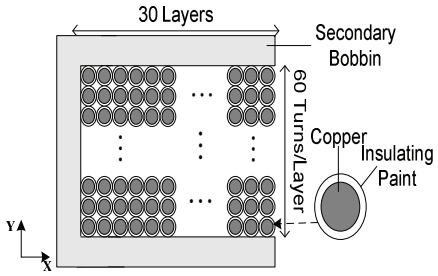

(b)

Fig. 1. Physical model of ignition coil, 1—Steel Core; 2—Primary Bobbin; 3—Secondary Bobbin; 4—Secondary Winding; 5—Primary Winding.

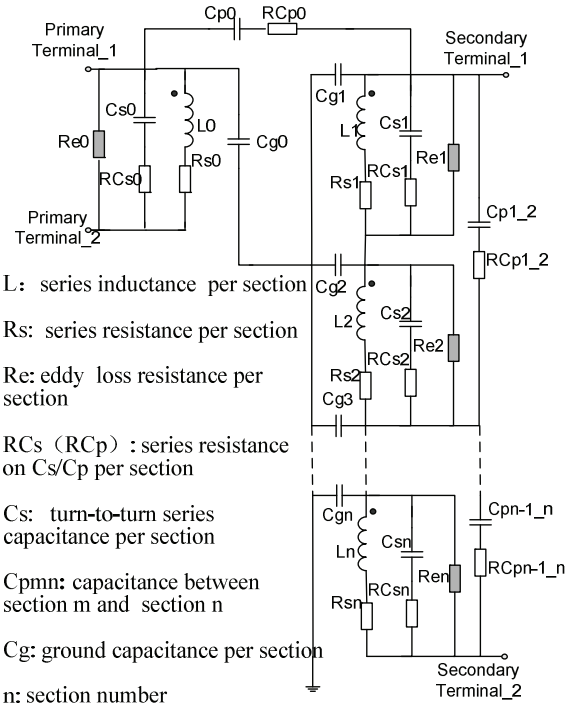

Fig. 2. Equivalent circuit model of ignition coil.

Figure 2 shows the equivalent circuit model. This model separates the winding into individual sections. Each section of the circuit consists of capacitance C, inductance L and resistance R. Ten sections were used in this model.

III. FEA CALCULATION FOR PARAMETERS

A. Capacitance Cg and Cpmn

For calculating the ground capacitance Cg and the section-to-section capacitance Cpmn, simplified solid winding substituted the real winding section, as shown in Fig. 3 (a). *l*, *w* is length and width of a winding section. Calculating the capacitance from FEA is related to the electrostatic energy W^e. The first step is to assign a voltage U_i to the winding section *i*; all other winding section in the volume V are grounded. FEA programme discretizes problem volume V into tetrahedral element, as shown in Fig. 3 (b) (205007 tetrahedrons in total), and then solves the Laplace equation to get the electric field $\mathbf{E}_i$ and the displacement field $\mathbf{D}_i$ according to (1).

$$\nabla\cdot(\varepsilon\nabla\Phi_i)=0;\ \mathbf{E}_i=-\nabla\Phi_i;\ \mathbf{D}_i=\varepsilon\mathbf{E}_i \qquad (1)$$

Where, Φ_i is the electric scalar potential. The same procedure is applied to other conductor *j* in succession; in the end, W^C_{ij} can be obtained from (2). The computation time is about 115 minutes (Memory 2GB, CPU Frequency 2.19GHz).

$$W^C_{ij}=\frac{1}{2}\int_V \mathbf{E}_i\cdot\mathbf{D}_j\,dV=\frac{1}{2}\int_V \mathbf{E}_j\cdot\mathbf{D}_i\,dV \qquad (2)$$

Since the energy can also be expressed

$$W^C_{ij}=\frac{1}{2}C_{ij}U_iU_j \qquad (3)$$

Further combining the (2) and (3), we can get C_{ij}, which is one element in capacitance matrix. When $i\neq j$, section-to-section capacitance Cp_{ij} is equal to C_{ij}; when $i = j$, ground capacitance Cg can be written as

$$Cg_i=C_{ij}-\sum_{i\neq j}C_{ij}. \qquad (4)$$

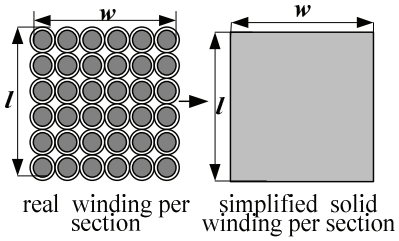

(a)

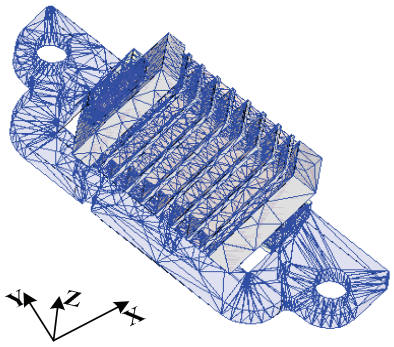

(b)

Fig. 3. Simplified solid model of real winding and 3D FEA mesh.

B. Capacitance Cs

For calculating the turn-to-turn series capacitance Cs of each winding section, the 3D geometry of each winding section is converted into an approximate 2D axis-symmetrical geometry. In this case, a simplified multi-layer sheet winding substitutes the real winding section, which omits the turn-to-turn capacitance in each layer of winding, as shown in Fig. 4 (a). The real winding is wound with round copper wire of diameter d_1 and overall wire diameter d_0; sheet winding is wound with rectangle conductor of length l and width u; h is the space between two layers. To guarantee that the cross-sectional area of the sheet winding is equal to that of the real winding, they have the following relations.

$$u = \frac{m\pi\left(\frac{d_1}{2}\right)^2}{l} \tag{5}$$

$$h = d_0 - d_1 \tag{6}$$

where m is the wire number in each layer of the real winding. FEA can be used to calculate the capacitance matrix, as mentioned in *A*, for the interaction between all the layers of sheet winding section. The computation time is about 3 minutes for each winding section. Figure 4(b) shows the triangular element when the layer number is 30 (25834 triangles in total). To this end, the electrostatic energy $W^C_{section}$ for a configuration of *N*-layer of winding, each excited with an applied potential, is given as

$$W^C_{section} = \frac{1}{2}\sum_{i=1}^{N}\sum_{j=1}^{N} C_{ij} U_i U_j \tag{7}$$

where U_i and U_j respectively represent the excited voltage to the layer i and the layer j of sheet winding. A modelling assumption is that the voltage difference (ΔU) between any two adjacent layer of winding is the same, so

$$U_i = i\Delta U, \quad U_j = j\Delta U \tag{8}$$

The stored energy $W_{section}$ can also be defined by the relation

$$W^C_{section} = \frac{1}{2} C_s U^2_{total} \tag{9}$$

where $U_{total} = (N-1)\Delta U$

Thus the series capacitance Cs in terms of all the layer-to-layer capacitance C_{ij} is

$$Cs(N) = \frac{\sum_{i}^{N}\sum_{j}^{N} ijC_{ij}}{(N-1)^2} \tag{10}$$

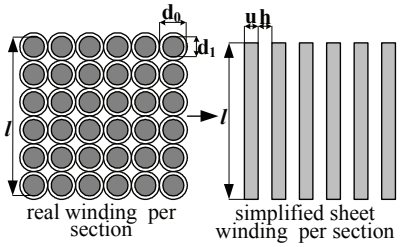

(a)

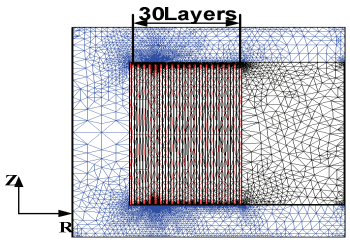

(b)

Fig. 4. simplified sheet model of real winding and 2D FEA mesh.

C. Inductance

In this work, the magnetic saturation phenomenon is ignored. Thus constant permeability μ, in the linear part of B-H curve, substitutes the varying steel property. The inductance of a set of winding sections can be calculated with the static magnetic store energy W^L, in analogy with the determination of capacitance from electric energy W^C. The procedure also depends on the FEA program to solve (11) for getting magnetic field $\mathbf{H}_i$ and magnetic flux density $\mathbf{B}_i$, which are corresponding to excitation with current I_i in winding section i, while the current excitations in the other winding section are zero. The same procedure is applied to other windings j in succession. The calculated energy in volume V can provide the self inductances (i=j) and mutual inductances ($i \neq j$), when combining (12) and (13). If the winding section i and j are, respectively, structured by N_i-turn and N_j-turn coil, the inductance L_{ij} can be obtained from (14).

$$\nabla \times \mathbf{H}_i = \mathbf{J}_i;\ \nabla \cdot \mathbf{B}_i = 0;\ \mathbf{B}_i = \mu \mathbf{H}_i \tag{11}$$

$$W_{ij}^{L} = \frac{1}{2}\int_V \mathbf{H}_i \cdot \mathbf{B}_j \, dV = \frac{1}{2}\int_V \mathbf{H}_j \cdot \mathbf{B}_i \, dV \tag{12}$$

$$W_{ij}^{L} = \frac{1}{2} L_{ij\_norm} I_i I_j \tag{13}$$

$$L_{ij} = N_i N_j L_{ij\_norm} \tag{14}$$

In reality, since the high frequency magnetic flux is difficult to enter inside the core of the transformer, the values of self and mutual inductances decrease as the frequency increases [8]. In order to study the impact of frequency on the magnetic flux, we adopted the magnetic scalar potential Ω in the whole domain and a current vector potential $\mathbf{T}$ in the conducting region to solve the eddy-problem. Applying Ampere's law, Faraday's law, and Gauss's law to the solenoidality of flux density yields two differential equations in conducting region as

$$\nabla \times \frac{1}{\sigma}(\nabla \times \mathbf{T}) = -j\omega\mu(\mathbf{T} - \nabla\Omega) \tag{15}$$

$$\nabla \cdot (\mu \mathbf{T}) = \nabla \cdot (\mu \nabla \Omega) \tag{16}$$

Here μ is the permeability, ω is angular frequency. In non-conducting region, the equation reduces to

$$\nabla \cdot (\mu \nabla \Omega) = 0 \tag{17}$$

The FEA program discretizes the problem region into tetrahedral elements, and by applying the Galerkin's approach, the discretized equation can be obtained [9]. After calculating the $\mathbf{T}$ and Ω of the nodal values, the magnetic flux density can be written as

$$\mathbf{B} = \mu(\mathbf{T} - \nabla\Omega) \tag{18}$$

In this work, we applied the unit current of 0Hz, 100Hz, 1kHz and 10kHz to the winding of the ignition coil. The magnetic lines of force in the core of the two-dimensional cross section are shown in Fig. 5; most of the magnetic line passes through the core when the frequency is 0Hz (static magnetic analysis) as shown in Fig. 5 (a); while as the frequency increases, the magnetic lines in the core significantly reduce when taking into account the skin effect and proximity effect, as shown in Fig. 5 (b), (c), and (d).

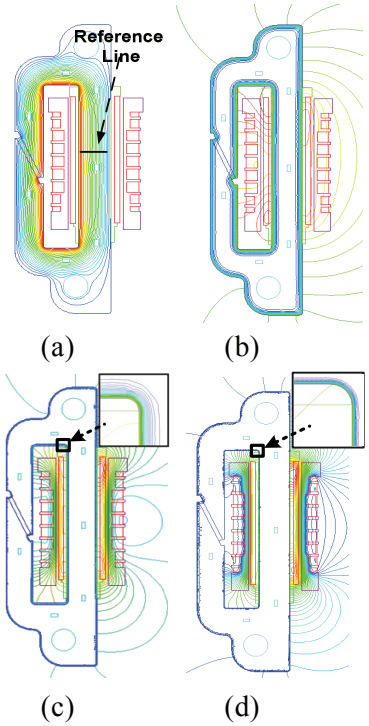

Fig. 5. Magnetic flux distribution of ignition coil at different frequencies at (a) 0Hz, (b) 100Hz, (c) 1kHz, and (d) 10kHz.

Figure 6 shows the flux as a function of core radius. B/B_{DC} is the relative value of static magnetic flux density on the reference line in

Fig. 5 (a); L/L_0 is relative position of the reference line; here, L_0 is the length of reference line. At 10kHz the magnetic flux within the transformer core is most completely displaced out of the core. Hence, when the frequency is above 10kHz, the core of ignition coil can be assumed as air or magneto-resistive material. In order to calculate the inductance matrix at low or high frequency with static magnetic analysis, relative permeability μ_r=2800 is defined for low frequency range, and the inductance matrix is defined as $\boldsymbol{L}_L$; while μ_r=0.001 is for high frequency range, and in this case the inductance matrix is defined as $\boldsymbol{L}_H$, as shown in Fig. 7.

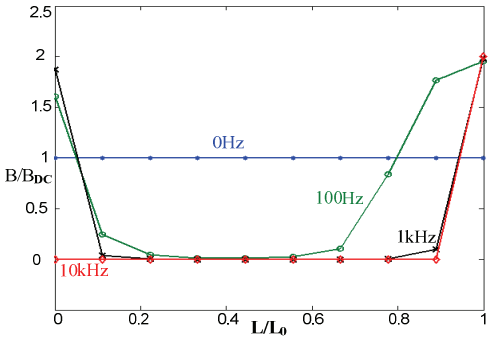

Fig. 6. Relative magnetic flux density value on the reference line.

D. Resistance

The winding resistance Rs/l =8.85Ω/m for the wire is used in this case. The effective resistance is expected to be larger because of the skin and proximity effect, but due to the small impact on the overall impedance of winding, this solution is considered sufficient. RCs/RCp represents the capacitance dielectric loss and its calculation equation is

$$RCs(f)/RCp(f) = \frac{tg\gamma}{2\pi fC} \qquad (20)$$

Here, tgγ is the dielectric loss tangent; C is the series capacitance value. In [6], the power factor of the capacitance circuit can be expressed by three different models, and the equivalent frequent point is determined by the intersection of power factor curves from the three models. The eddy current loss resistance Re is calculated based on [10], which does not generally change the overall shape of impedance curve of winding, but only influence the maximum limits.

IV. SIMULATION AND EXPERIMENT

A. Frequency-Domain

To investigate the secondary winding terminal impedance response from 100Hz to 10MHz, the following simulation cases were studied: Case (A), low frequency inductance matrix LL is adopted as series inductance L; Case (B), high frequency inductance matrix LH is adopted as series inductance L; Case (C), ignoring the turn-to-turn series capacitance Cs. As shown in Fig. 8, in case (A), the simulation matches well with the measurement from 100Hz to 10MHz. In case (B), the simulation partly agrees with the measurement from 80kHz to 10MHz. From the plots of case (A) and (B), inductances of winding convert from the LL to LH above 80 kHz; but the plot of (A), adopting the LL, agrees well with the measurement in the whole frequency domain; this phenomenon shows that the inductance does not influence the overall impedance in high frequency. In case (C), the simulation partly agrees with the measurement from 100Hz to 15kHz, which means the impedance of ignition coil above 15kHz is mainly decided by the capacitance of the winding. The measured data was got by impedance analyzer-Agilent4294A.

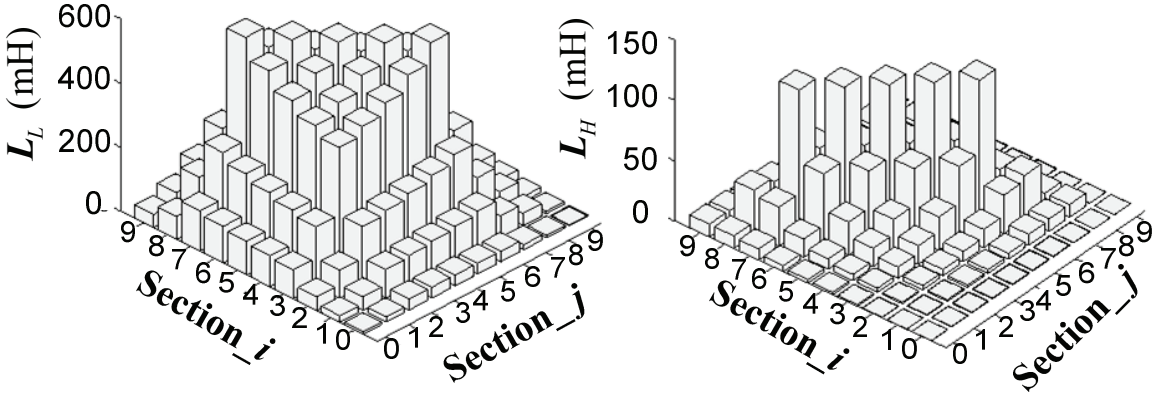

Fig. 7. Inductance Matrix in low-frequency (left) range and high frequency range (right).

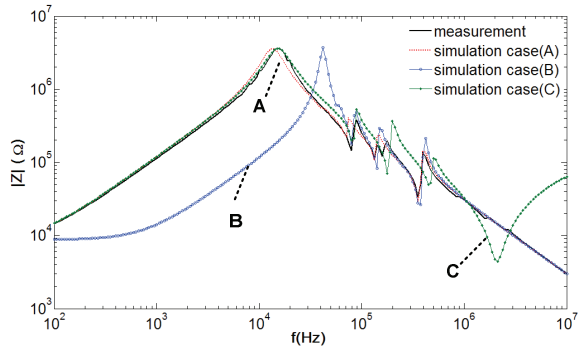

Fig. 8. Measured and simulated magnitudes of secondary winding impedance.

B. Time-Domain

In time-domain simulation, we used the case (A) to investigate the transient response of ignition coil. Fig.9 shows the transient voltage test circuit principle. The test equipments include: High-voltage probe Tektronix P6015A, Current probe Agilent 1146A, Oscilloscope Tektronix MSO 4032 and Waveform generator Agilent 33220A.

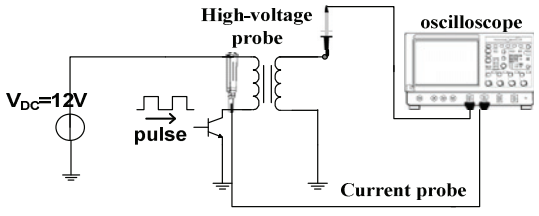

Fig. 9. Time-domain test circuit principle of ignition coil.

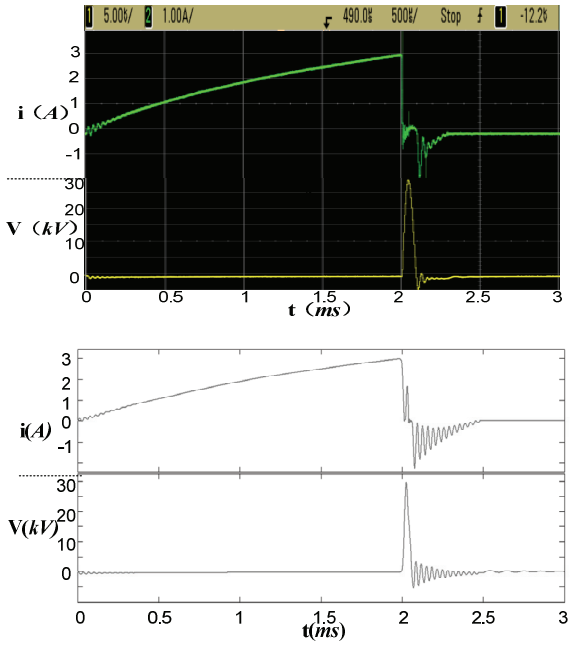

Fig. 10. Measured (upper) and simulated (lower) current of primary winding and voltage of secondary winding.

The primary winding current and secondary winding voltage are measured and simulated, as shown in Fig. 10. At t=0ms, at the opening of the switch device, the primary current waveform and secondary voltage waveform have small oscillation due to the inductance and capacitance in the ignition coil. In the interval 0ms < t < 2ms, the primary current is approximately linearly increasing to maximum value of 3A, and the

secondary voltage switches to zero. At t=2ms, at the closing of the switch device, the high changing rate of primary current induces high-voltage pulse of amplitude of 30kV in secondary winding. And for t>2ms, the primary current shows damped ringing around average value of -1A, while the secondary voltage shows damped ringing around average value of 0V. The simulation agrees well with the main part of waveform of the measurement.

V. CONCLUSION

This paper presented an equivalent lumped circuit model for predicting the wideband characteristic of automotive ignition coil. The main parameters in the circuit were calculated with FEA. In addition, FEA provides the approach to analysis the impact of frequency on the magnetic flux in the core. This circuit model was validated by experiment in both frequency and time domains, and those simulations agreed well with measurements.

ACKNOWLEDGEMENT

This work was supported in part by the National Natural Science Foundation of China (No. 50877081) and in part by the Third Stage Training of the "211 Project" of Chongqing University (No. S-09111).

REFERENCES

[1] B. Rohwein and B. Camilli, "Advanced automotive ignition system", *Digest of Technical Papers-IEEE International Pulsed Power Conference,* vol. 1, pp. 40-45, 1995.

[2] P. Ying, R. Jiangjun, Z. Yu, et al., "Calculation of very fast transient voltage distribution in pulse transformer", *Proceedings of the CSEE,* vol. 25, no. 11, pp. 140-145, 2005.

[3] M. Popov, L. van der Sluis, and. J. L. Roldan, "Analysis of Very Fast Transients in Layer-Type Transformer Windings", *IEEE Transactions on Power Delivery,* vol. 22, no. 1, pp. 238-247, 2007.

[4] J. Biernacki and D. Czarkowski, "High Frequency Transformer Modeling", *IEEE International Symposium on Circuit and Systems,* vol. 3, pp. 676-679, 2001.

[5] M. A. Eldery, Saadany, and Salama, "Parameters Identification of Sectional Wingding High Frequency Transformer Model Using Neural Network", *IEEE International Symposium on Micro-Nanomechatronics and Human Science,* vol. 2, pp. 974-977, 2005.

[6] M. T. Yoshikazu and T. Teranishi, "Modeling and Analysis of Transformer Winding at High Frequencies", *The International Conference on Power Systems Transients (IPST05),* 2005.

[7] M. Wang, A. John Vandermaar, and K. D. Strivastava, "Improved Detection of Power Transformer Winding Movement by Extending the FRA High Frequency Range", *IEEE Transactions on Power Delivery,* vol. 20, no. 3, pp. 1930-1938, 2005.

[8] A. M. Miri, N. A. Riegel, and Andreas, "Finite Element Models For the Computation of the Transient Potential and Field Distribution in the Winding System of High Voltage Power Transformers," *IEE Conference Publication,* vol. 2, pp. 467, pp. 39-42, 1999.

[9] P. Zhou,W. N. Fu, D. Lin, S. Stanton, and Z. J. Cendes, "Numerical modeling of magnetic devices," *IEEE Trans. Magn.*, vol. 40, pp. 1803–1809, July 2004.

[10] J. Benecke and S. Dickmann, "Analytical HF Model for Multipole DC Motors", *Proceedings of the 18th international Zurich Symposium on Electromagnetic Compatibility,* pp. 201-204, 2007.

Jia Jin was born in Si Chuan Province, China in 1985. Since 2007, he has been pursuing his M.S degree at the college of electrical engineering in Chongqing University, China. His areas of interest are electro-magnetic computation and electromagnetic compatibility.

Wang Quandi was born in Anhui province, China in 1954. She received her Ph.D degree from the College of Electrical Engineering of Chongqing University, Chongqing, China, in 1998. Currently, she is a professor in the college of Electrical Engineering, Chongqing University. Her main research interests are simulation and numerical computation of electromagnetic fields.

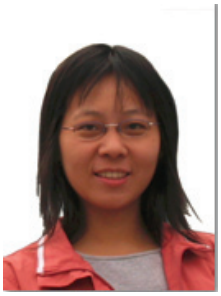

Zheng Ya-li was born in Henan Province, China in 1982. She received the B.S. degree in electrical engineering from Chongqing University, Chongqing, China, in 2005, where she is pursuing her Ph.D. degree in electrical engineering. Her research interests include electromagnetic computation, electromagnetic compatibility and transmission-line analysis.

Yu Jihui was born in Changsha, Hunan province, China in 1944. Now, he is Professor of the College of Electrical Engineering at Chongqing University in China. His main research interests are the numerical computation and simulation of electromagnetic fields and electromagnetic compatibility, and also in the information management system field.